J Sol-Gel Sci Technol (2015) 75:366–373
DOI 10.1007/s10971-015-3709-1

ORIGINAL PAPER

Modified photodeposition of uniform Ag nanoparticles on TiO_2 with superior catalytic and antibacterial activities

Jianqi Ma[1,2] · Shaobo Guo[2] · Xiaohua Guo[1] · Hongguang Ge[1]

Received: 22 January 2015 / Accepted: 9 April 2015 / Published online: 19 April 2015

Abstract Photocatalytic reduction is a facile and effective route to deposit Ag nanoparticles (NPs) on TiO_2. Nevertheless, it is difficult to produce Ag NPs that have small particle size and uniform distribution on TiO_2 to form core–shell structure TiO_2@Ag composites by straightforward photodeposition. In this study, monodisperse TiO_2 spheres composed of anatase nanocrystals were directly employed as templates to deposit small and homogeneously dispersed Ag NPs by modified photodeposition procedure. To prove the feasibility of the innovative method, we evaluated the catalytic performance and bactericidal efficacy of the as-prepared samples based on the characterizations, since there is strong dependence between size and dispersion of Ag NPs and catalytic performance and inhibition of bacterial growth, where smaller and more highly dispersed Ag NPs displayed better antimicrobial and catalytic properties. The results indicate that the modified photodeposition route can effectively prevent TiO_2 spheres themselves from aggregating and Ag NPs from rapid overgrowing on the TiO_2 surface in the deposition process. The superior bactericidal and catalytic properties of the TiO_2@Ag composites are largely attributed to the small and highly dispersed Ag NPs on TiO_2 spheres.

Graphical Abstract

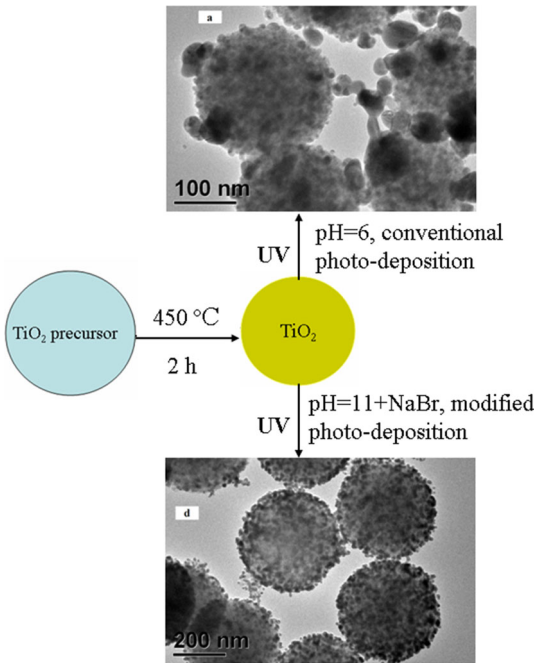

Keywords Photodeposition · TiO_2@Ag composites · Catalytic performance · Antibacterial activity

1 Introduction

Noble metal NPs exhibit completely new or improved properties based on specific characteristics such as size, distribution and morphology in comparison with their bulk counterparts [1–6]. Ag NPs have been studied intensively for their potential use in catalysis, biosensors, biomedicine and environmental filtration due to their unique optical and electrical properties and excellent antibacterial activity

✉ Jianqi Ma
jianqima@163.com

[1] School of Chemistry and Environmental Science, Shaanxi University of Technology, Chaoyang Road, Hanzhong 723001, China

[2] School of Biological Science and Engineering, Shaanxi University of Technology, Hanzhong 723001, China

[7–12]. It is well known that the high surface energy of the Ag NPs makes them easily aggregate to big particles, which could deteriorate their unique chemical properties and induce loss of overall performance. Therefore, the stability is one of the most important factors for their practical applications in nanoscience and nanotechnology. To stabilize Ag NPs, an efficient measure is to immobilize highly dispersed Ag NPs on inexpensive substrates such as SiO_2, Fe_3O_3, ZnO, ZrO_2, CeO_2, Al_2O_3, C materials and TiO_2 [13–31]. Particular attention has been focused on supporting and binding AgNPs onto TiO_2 surface to improve catalytic and photocatalytic performance, and antimicrobial activity due to the synergistic interaction between Ag NPs and TiO_2 support [20–28]. Moreover, the assembly of Ag NPs on the support could enhance their stability and easy separation from the reaction medium for recycle. Photodeposition is a facile and effective method to deposit various noble metal NPs on the surface of TiO_2 under UV light. Nevertheless, it is difficult to produce uniform Ag NPs that have very small size and are strongly anchored on the surface of TiO_2 by conventional photodeposition [29–31].

In this study, monodisperse TiO_2 spheres composed of anatase nanocrystals were directly employed as templates to deposit small and homogeneously dispersed Ag NPs by modified photodeposition procedure. To prove the feasibility of the innovative method, we evaluated the catalytic performance and bactericidal efficacy of the as-prepared samples based on the characterizations.

2 Experimental

2.1 Chemicals

Titanium tetraisopropoxide (TTIP, purity $\geq$ 97 %) is purchased from Sigma-Aldrich. $AgNO_3$ (purity $\geq$ 99.9 %), methylamine (MA, 40 % aqueous solution), rhodamine B (Rh B, purity $\geq$ 99.0 %), sodium borohydride ($\geq$99.0 %), methanol, ethanol and acetonitrile are of analytical grade and purchased from Shanghai Chemicals Co., Ltd., China, and used without any further purification. Gram-negative bacteria *Escherichia coli* (*E. coli*, ATCC 25922) and Gram-positive bacteria *Staphylococcus aureus* (*S. aureus*, ATCC 6538) were purchased from Guangdong Institute of Microbiology. Deionized water was used throughout the experiments except for in the antibacterial tests where sterilized H_2O was used.

2.2 Preparation of TiO_2, TiO_2/Ag and TiO_2@Ag composites

The monodisperse TiO_2 spheres were synthesized according to the reported procedures with some modifications [32]. In a typical procedure, 6.0 mmol TTIP stabilized in 10 mL anhydrous ethanol was dropwise added into a premixed solution of 50 mL ethanol and 40 mL acetonitrile containing 1.2 mmol MA and 24 mmol H_2O. The solution turned milky within a few seconds, and the prepared suspension was stirred for 6 h to form the amorphous TiO_2 spheres. The white precipitate was harvested by centrifugation, followed by washing with ethanol five times and drying at 60 °C for 24 h. The dried powders were calcined at 450 °C for 2 h in air to remove organic components and transform the amorphous precursors into anatase TiO_2 spheres for further use.

Two different deposition processes, one is conventional photodeposition for TiO_2/Ag composites and the other is modified photodeposition for TiO_2@Ag composites, were conducted in a photochemical reactor as we adopted previously [33]. In the two cases, Ag-coated TiO_2 samples with Ag/Ti molar ratio = 8 % (the same depositing amount of Ag on TiO_2) were prepared. For conventional photodeposition, suspension was prepared by ultrasonic mixing 100 mg (1.25 mmol) of TiO_2 and 15.8 mg (0.093 mmol) of $AgNO_3$ with 180 mL of ultrapure water and 20 mL of methanol in the Pyrex glass reactor. The suspension was purged with a stream of N_2 for 30 min to remove oxygen and then irradiated for 4 h at under N_2 and magnetic stirring. The black precipitate was recovered by centrifuging and washing five times, dried at 60 °C for 24 h.

The modified photodeposition was carried out in the same manner as described above, except for that the pH of the suspension was adjusted to 11 and a predetermined amount of NaBr was added into the suspension.

2.3 Characterization of samples

The XRD patterns were obtained on a Bruker D8 Advance X-ray diffractometer with Cu-Kα radiation (λ = 0.15418 nm). The observation of the morphology was performed on a JEOL JEM-2010 TEM at acceleration voltage 200 kV. The UV–visible absorption spectra were measured using a Hitachi U-3010 UV–Vis spectrophotometer. XPS study was carried out on a PHI-5702 multifunctional X-ray photoelectron spectroscopy, using MgKα radiation as the excitation source and the binding energy of contaminated carbon (C1s 284.6 eV) as the reference, at a pass energy of 29.4 eV and a resolution of ±0.2 eV in the binding energy position.

2.4 Catalytic performance

The catalytic degradation of Rh B was carried out in a quartz cuvette with an optical path length of 1 cm at room temperature. 1.0 mL of aqueous Rh B solution

(2×10^{-5} mol/L) was mixed with 1.0 mL of a fresh $NaBH_4$ solution (0.01 mol/L). 0.2 mL of aqueous dispersion of TiO_2, TiO_2/Ag and TiO_2@Ag composites (0.03 %) was added separately. The color of the mixture was fading with the experiment proceeding, indicating a gradual reduction of Rh B. The catalytic performance was studied by monitoring the variation in optical density at the wavelength of the absorbance maximum (λ_{max}) of the dye with UV–Vis.

2.5 Antibacterial activity

The antibacterial activity of the as-prepared samples against *E. coli* and *S. aureus* were evaluated using paper disk diffusion assay [19] and spread-plate method on LB agar spread onto a Petri plate [21, 34], respectively, with some modifications. The disk diffusion assay was performed by placing a 7-mm filter paper disk saturated with different concentrations of pure TiO_2, TiO_2/Ag and TiO_2@Ag composite spheres (0.25, 0.5, 0.75 and 1.0 g/mL, respectively) onto agar plates (4 per plate) seeded with 10^5 CFU (colony forming units) of *E. coli* and *S. aureus*, respectively. After incubation at 37 °C for 24 h, the diameters of the inhibition zones were observed and measured. The paper disk saturated with sterilized water was used as the control. To use spread-plate method, the tested bacterial suspension (an aqueous suspension of bacteria/antimicrobial agents) was prepared with 1×10^3 CFU/mL of *E. coli* and *S. aureus* containing 0.25 mg/mL TiO_2, TiO_2/Ag and TiO_2@Ag composites, respectively. Out of each sample, 0.1 mL of the suspension was spread over LB agar plates, which were then incubated at 37 °C for 24 h in the dark. Control experiment with only bacterial suspension without antimicrobial agents was conducted to quantify the CFU of bacterial strain in the blank sample.

3 Results and discussion

3.1 Characterization

Figure 1 shows typical TEM images of the amorphous TiO_2 precursors and the anatase TiO_2 spheres. It can be seen that amorphous TiO_2 spheres are highly monodispersed with average size of 210 nm and possess very smooth surfaces without obvious granular feature (Fig. 1a). After heat treatment at 450 °C for 2 h, the anatase TiO_2 spheres still keep the original monodisperse morphology, the average size of the particles was reduced to 185 nm (15 % shrinkage), and comparatively rough surfaces with granular feature were produced (Fig. 1b).

A simple suspension of anatase TiO_2 spheres containing $AgNO_3$, without pH adjustment (pH 6) and other chemical additives, was straightforwardly exposed to ultraviolet irradiation. The representative TEM image of the as-prepared sample is shown in Fig. 1c. It is found that the sizes of the Ag NPs deposited on the TiO_2 are large and heterogeneously dispersed, and TiO_2 spheres tend to have a certain degree of aggregation. No real core–shell structure TiO_2@Ag has been formed, and we designate it as TiO_2/Ag. In the case, Ag^+ adsorbed onto the exposed TiO_2 surfaces is photochemically reduced to initially form metal nucleus centers, which can act as the reservoir of photoinduced electrons to accelerate the photoreduction of Ag^+ ions. The Ag deposits with large size and wide size distribution should be attributed to their rapid overgrowth on the original TiO_2 particles. On the other hand, the pH employed is near the isoelectric point (IEP = 6.25) of TiO_2 [35, 36] and might cause the aggregation of the TiO_2 particles [30]. The stability of TiO_2 spheres in suspension is influenced by pH values. If the pH value of suspension is higher or lower than the IEP of TiO_2, the TiO_2 surface will be negatively or positively charged, respectively. The further the pH value is from the IEP, the more stable and the better dispersed TiO_2 particles will be. Oppositely, if close to or equal to the IEP, TiO_2 particles will be aggregated.

When the pH of the suspension was adjusted to 11 and a predetermined amount of NaBr was added into the suspension, most of Ag^+ in the forms of insoluble Ag_2O and soluble $AgNO_3$ can be transformed into insoluble AgBr due to the difference in solubility product constant K_{sp} [$K_{sp}(AgBr) = 5.0 \times 10^{-13}$, $K_{sp}(AgOH) = 2 \times 10^{-8}$]. As shown in Fig. 1d, the monodispersed Ag NPs with average size of 8 ± 1.5 nm, uniform spherical shape and narrow size distribution are homogeneously deposited on TiO_2 surfaces to form core–shell structured TiO_2@Ag composites. This is in perfect consistency with the hypothesis that lower concentration of free Ag^+ on the TiO_2 surface and in bulk solution is very effective in producing small and highly dispersed Ag NPs on TiO_2. Both nucleation kinetics and growth kinetics of metal will influence the morphology and size distribution of deposited Ag NPs. The simultaneous nucleation on different active sites and slow growth of these metal nuclei are preferred for the preparation of homogeneously dispersed metal NPs with sharp size distribution. It can be easily understood that if the growth of metal nucleus is too fast, minute diversity of nucleation rate on different active sites in the initial stage of irradiation will cause great growth difference in nucleus. The former deposited nucleus, acting as electron reservoir to inhibit the recombination of photoinduced electrons, can accelerate the growth of metal particles and become big more rapidly than those latter deposited nuclei, which broadens the resultant size distribution of metal particles. An anticipated way to weaken the influence of nucleation kinetics and growth kinetics of metal particles is to keep

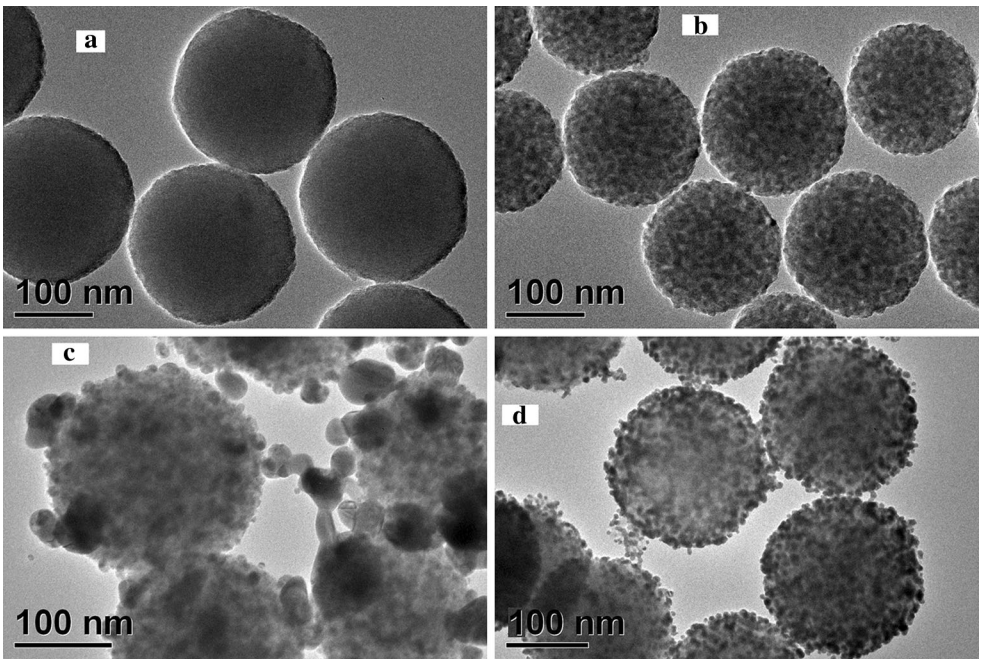

Fig. 1 TEM images of **a** amorphous TiO_2 precursor spheres, **b** anatase TiO_2 spheres, **c** TiO_2/Ag and **d** TiO_2@Ag composites

the local concentration of Ag ions on the TiO_2 surface and the bulk concentration of Ag ions in the suspension extremely low. In addition, in this case, the pH value is far from the IEP of TiO_2 to assure the TiO_2 well dispersed which inhibited the aggregation of Ag NPs. Therefore, the procedure can effectively prevent TiO_2 spheres themselves from aggregating and Ag NPs from rapid overgrowing on the TiO_2 surface in the photodeposition process, thus resulting in more dispersed and smaller-sized Ag NPs on TiO_2 compared to conventional photodeposition method.

To confirm the existed states of Ag coated on TiO_2, both the TiO_2/Ag and the TiO_2@Ag composites with the same Ag loading were characterized by XRD and XPS. Figure 2 shows the XRD patterns of TiO_2 spheres, TiO_2/Ag and TiO_2@Ag composites, respectively. The powder XRD pattern of the pure TiO_2 exhibits well-resolved diffraction peaks (Fig. 2a), corresponding to the reflections of anatase TiO_2 (JCPDS card 21-1272). Compared to Fig. 2a, both the TiO_2/Ag (Fig. 2b) and TiO_2@Ag composites (Fig. 2c) exhibit four additional peaks at 2θ angles of 38.1°, 44.2°, 64.4° and 77.4° corresponding to the reflections of (111), (200), (220), (311) and (222) crystalline planes of face-centered cubic metallic silver (JCPDS card 04-0783), respectively. One can see the intensity of the corresponding anatase peaks was reduced when Ag NPs were deposited on TiO_2. Meanwhile, the peak intensity in the 2θ region of 36°–40° significantly enhances because both characteristic diffraction peaks of 38.1° of Ag crystals and 38.6° of anatase TiO_2 overlap. However, it can be clearly seen that the XRD peaks of Ag crystals in the TiO_2@Ag composites

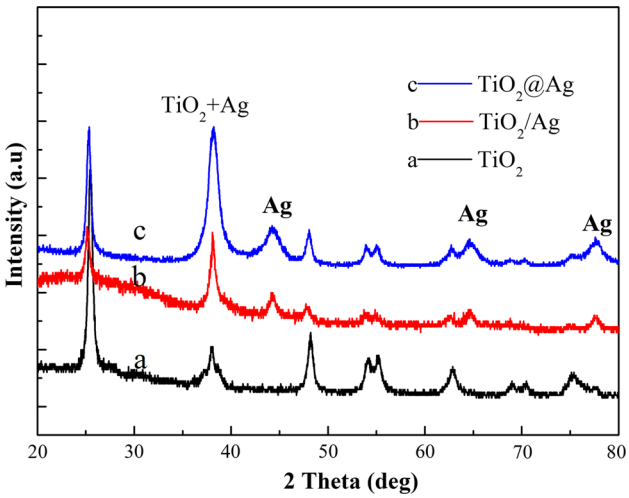

Fig. 2 XRD patterns of *a* anatase TiO_2 spheres, *b* TiO_2/Ag composites and *c* TiO_2@Ag composites

(Fig. 2c) are slightly wider than that in the TiO_2/Ag composites (Fig. 2b), indicating that the former has smaller Ag particle size than the latter. The results are consistent with TEM analysis. To further investigate the possible chemical status of Ag (Ag^0 or Ag^+) in TiO_2@Ag composites, the corresponding high-resolution XPS spectrum of Ag 3*d* is shown in Fig. 3. The photoelectron peaks of both the Ag $3d_{5/2}$ and Ag $3d_{3/2}$ are basically symmetrical with binding energy (BE) of 368.3 and 374.2 eV, respectively, and the 6.0 eV difference between the BE of Ag $3d_{5/2}$ and Ag $3d_{3/2}$ peaks is also characteristic of metallic Ag 3*d* states. The

results prove that Ag exists in form of metallic Ag in the composites [21–30]. Combined with the results of XRD analysis, it can be concluded that Ag particles are not oxidized in the photodeposition process under UV irradiation.

The UV–Vis absorption spectra of pure TiO_2, TiO_2/Ag and TiO_2@Ag composites are illustrated in Fig. 4. It can be seen that neat TiO_2 spheres have a broad intense absorption below 400 nm. It is the characteristic absorption of TiO_2 corresponding to the charge transfer process from the valence band to conduction band in anatase TiO_2 [37–40]. The photodeposited Ag NPs cause significant changes to the absorption spectrum of TiO_2, resulting in high absorbance from 400 nm to entire visible region, which is characteristic of surface plasmon absorption corresponding to deposited metallic Ag NPs on TiO_2 surfaces [21–29]. The absorbance in the visible region increased firstly and then decreased gradually from 400 to 800 nm for the TiO_2/Ag composites, indicating that Ag NPs on TiO_2 are not evenly distributed [40]. In contrast, the TiO_2@Ag composites prepared by the modified deposition route basically maintain constant absorption in the visible region, corresponding to uniformly distributed Ag NPs on TiO_2.

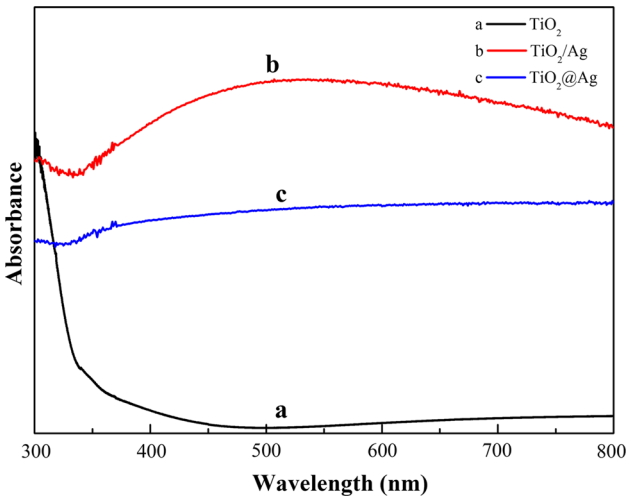

Fig. 4 UV–Vis spectra of *a* anatase TiO_2 spheres, *b* TiO_2/Ag composites and *c* TiO_2@Ag composites

3.2 Catalytic performance

The catalytic degradation of Rh B was chosen as a model reaction to investigate the catalytic performance of both the TiO_2/Ag and the core–shell structure TiO_2@Ag composites. Such a reaction catalyzed by Ag catalysts has been reported because this reaction can be rapidly and easily characterized [13, 41]. The absence of catalyst but in the presence of KBH_4 in the Rh B solution only results in a slight decrease in λ_{max} after standing for 10 h (results not shown here), indicating that the reduction does not proceed without catalyst. Nevertheless, there was no obvious change in the intensity at 554 nm after 20 min when TiO_2 was added to the above mixture (Fig. 5a), indicating that it is inactive toward the catalytic degradation of RhB with bare TiO_2 spheres as catalyst [42]. Figure 5b shows the UV–Vis spectra monitoring the catalytic reduction of RhB, measured at different times using TiO_2/Ag composites as the catalyst. The absorption peak at 554 nm gradually decreased in intensity and ultimately vanished as the reaction proceeded for 20 min, confirming that the reduction is mainly catalyzed by the Ag NPs on TiO_2. Instead of TiO_2/A g, TiO_2@Ag composites were added, the absorption intensity at 554 nm dramatically and quickly decreased and disappeared after 8 min (Fig. 5c). This indicates that the catalytic efficiency of TiO_2@Ag composites is much higher than TiO_2/Ag composites.

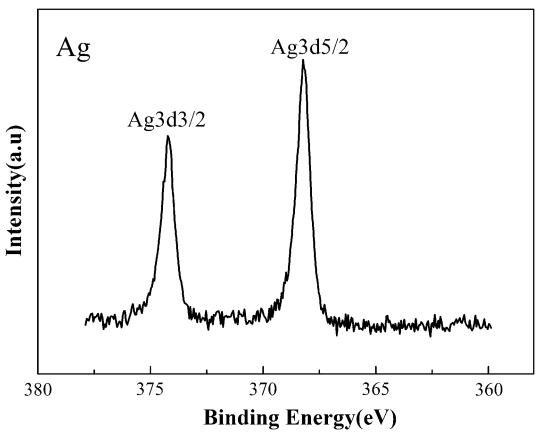

Fig. 3 High-resolution XPS spectrum of Ag 3*d* in TiO_2@Ag composites

3.3 Antibacterial property

First, the antibacterial activity of the as-prepared samples was investigated by measuring the growth inhibition of the bacteria on solid agar plates through paper disk diffusion assay method. In the disk diffusion assay experiment, the paper disks were saturated with different concentrations of TiO_2 spheres, TiO_2/Ag and TiO_2@Ag composites, which were placed on LB agar plates and seeded with *E. coli* and *S. aureus*. Subsequently, these plates are incubated at 37 °C for 24 h, and then, the antibacterial effects are evaluated by measuring the diameter of inhibition zone. As shown in Fig. 6a, b, comparing with the blank control groups (a_0–d_0), the TiO_2 spheres (a_1–d_1) have almost no antibacterial activity against the both bacteria. When Ag NPs photodeposited on TiO_2, the zones of inhibition can be clearly observed and the growth of the *E. coli* cells and *S. aureus* is significantly inhibited in the presence of both the

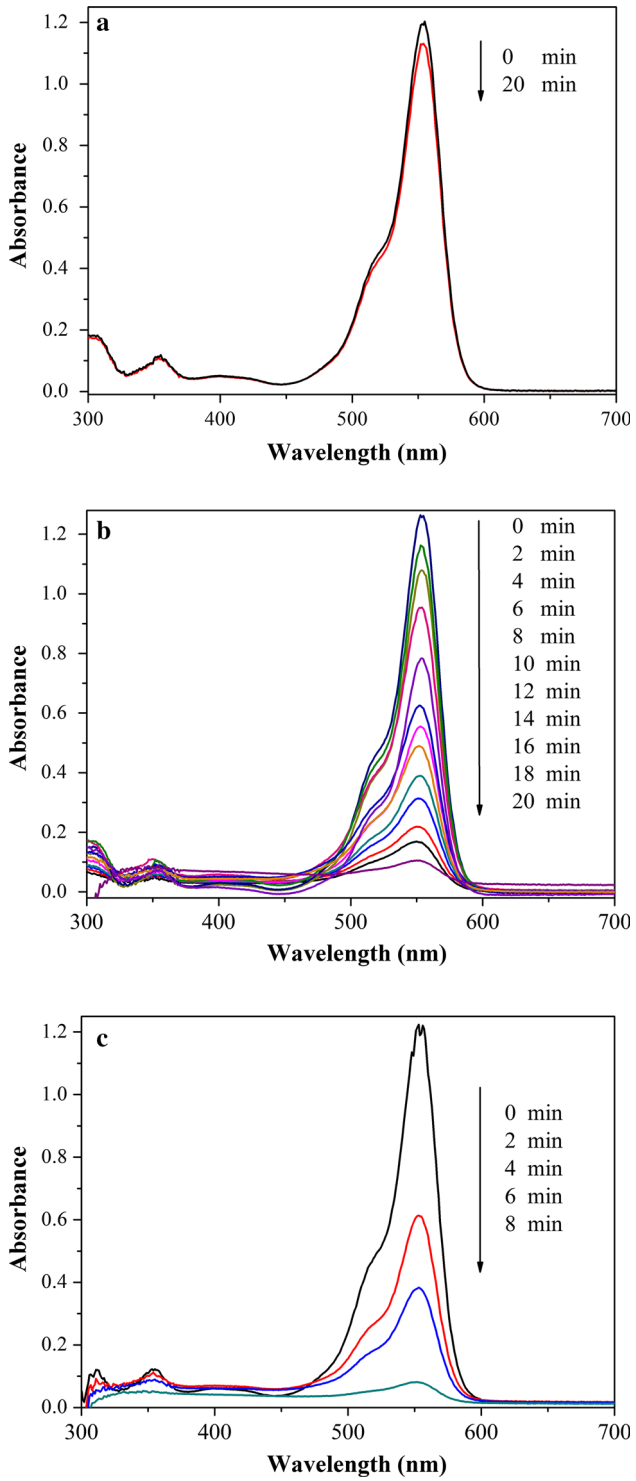

Fig. 5 Evolution of the absorption spectra of Rh B solution (10 mg/L) in the presence of **a** pure TiO_2, **b** TiO_2/Ag composites and **c** TiO_2@Ag composites

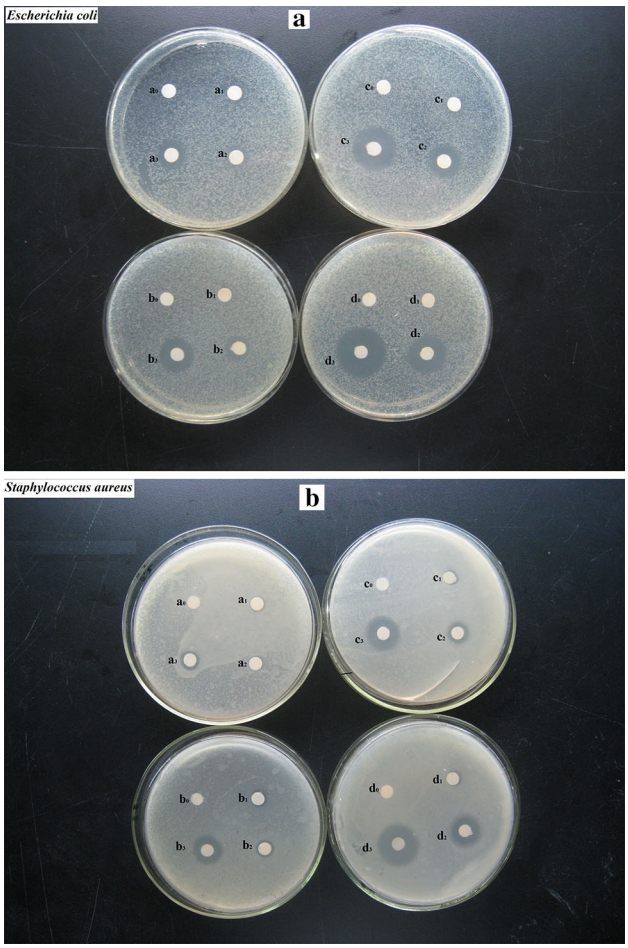

Fig. 6 Inhibition zones of the as-synthesized TiO_2 spheres, TiO_2/Ag composites and TiO_2@Ag composites against **a** *E. coli* and **b** *S. aureus*. Control groups saturated with sterilized water (a_0–d_0). Experimental groups saturated with 0.25, 0.5, 0.75 and 1.0 mg/mL of TiO_2 spheres (a_1–d_1), TiO_2/Ag (a_2–d_2) and TiO_2@Ag (a_3–d_3) composites, respectively

TiO_2/Ag (a_2–d_2) and TiO_2@Ag (a_3–d_3), even at very low concentration (0.2 mg/mL). Moreover, with their concentrations increasing gradually, the inhibition zones grow larger. However, the inhibition zone diameters of the TiO_2/Ag spheres are obviously smaller than that of the TiO_2@Ag composite spheres at the same concentration. The results reveal that TiO_2@Ag composites exhibit higher antibacterial efficiency than TiO_2/Ag.

The bactericidal activity was further confirmed using spread-plate method by the images of colonies on agar plates. Figure 7a, b presents the results of the antibacterial tests using 0.2 g/mL pure TiO_2, TiO_2/Ag and TiO_2@Ag composites against *E. coli* and *S. aureus* on LB agar plates, respectively, after 24-h incubation. A comparison between the blank (Fig. 7Aa, Ba) and the TiO_2 (Fig. 7Ab, Bb) shows that pure TiO_2 particles exhibit extremely weak bacteriostatic action [21]. About 11 % *E. coli* and 24 % *S. aureus* survive in the presence of TiO_2/Ag (Fig. 7Ac, 7Bc), and TiO_2@Ag composites lead to almost complete suppression of *E. coli* and *S. aureus* growth (Fig. 7Ad, Bd). The antibacterial tests performed on the two Ag-modified

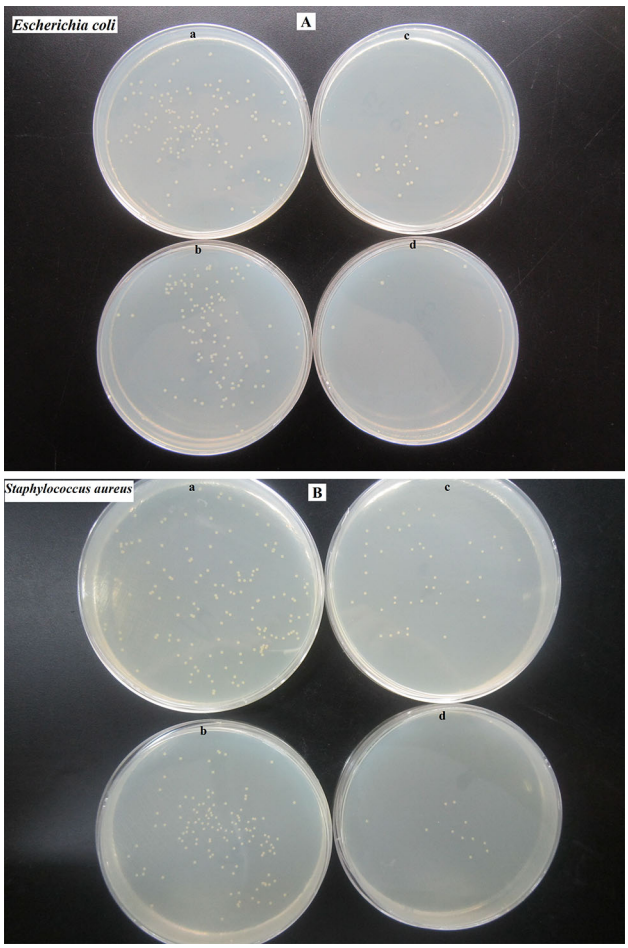

Fig. 7 Spread-plate test results using 0.2 mg/mL of TiO_2, TiO_2/Ag and TiO_2@Ag composites against **A** *E. coli* and **B** *S. aureus.* (*a*) Blank, (*b*) pure TiO_2, (*c*) TiO_2/Ag composites, (*d*) TiO_2@Ag composites

samples showed a much greater activity toward *E. coli* than *S. aureus* due to different cell wall structures and different antibacterial mechanisms of Ag NPs against different cells [34]. Several mechanisms for their bactericidal effects have been proposed, it is widely believed that Ag NPs are incorporated in the cell membrane, which causes leakage of intracellular substances and eventually causes cell death. Gram-negative strains such as *E. coli* have a thinner wall in comparison with Gram-positive ones (i.e., *S. aureus*), and it is difficult for Ag NPs to penetrate the thicker cell wall of *S. aureus* due to its higher resistance. However, TiO_2@Ag composites possess higher antibacterial efficiency against *E. coli* and *S. aureus* than TiO_2/Ag. The significantly different bactericidal activity between the two samples was largely attributed to the difference in the Ag particle size and distribution. The smaller Ag particle size and highly dispersed Ag NPs firmly attached onto TiO_2 sphere surfaces should account for the higher antibacterial activity of TiO_2@Ag. The dependence on particle size and distribution of antibacterial activity can be understood from three aspects: (1) Smaller particles have more surface atoms that are expected to be active upon contact with bacterial cells; (2) smaller particles also have a larger fraction of atoms on low-coordination and high-energy sites, which makes them more active than larger particles; (3) the number of Ag particles uniformly distributed on TiO_2 sphere surfaces is more than un-uniformly distributed counterparts at the same silver load, and their exposed surface areas differ significantly as well. This unique core–shell structure of TiO_2@Ag composites could more effectively promote Ag/bacteria contact and thus enhanced bactericidal efficiency in attacking and destructing bacterial cell membranes.

4 Conclusions

Core–shell structure TiO_2@Ag composites have been synthesized using modified photodeposition route, i.e., the pH of the suspension of TiO_2 and $AgNO_3$ was adjusted to 11 and a certain amount of NaBr (equal molar to $AgNO_3$) was added into the suspension to transform Ag^+ into the corresponding AgBr. The highly dispersed TiO_2 spheres can serve as a rigid scaffold to prevent the Ag NPs from aggregating during the reaction. A smaller particle size and more uniform particle distribution result in a larger surface-to-volume ratio and more exposed atoms on surface as potential active sites. This core–shell structural feature is favored for enhancing the catalytic and antibacterial properties compared with TiO_2/Ag composites in that the latter tend to suffer from the loss of activity due to aggregation. The present method is versatile, and other noble metals including Au, Pd, Pt and their bimetallic NPs can also be evenly loaded onto the surfaces of TiO_2 spheres by the modified photodeposition procedure according to their respective properties.

Acknowledgments This work was supported by the National Natural Science Foundation of China (No. 21373132).

References

1. Lu YZ, Chen W (2012) Chem Soc Rev 41:3594–3623
2. Yin YD, Alivisatos AP (2005) Nature 437:664–670
3. Sau TK, Rogach AL (2010) Adv Mater 22:1781–1804
4. Millstone JE, Hurst SJ, Metraux GS, Cutler JI, Mirkin CA (2009) Small 5:646–664
5. Song SY, Liu RX, Zhang Y, Feng J, Liu DP, Xing Y, Zhao FY, Zhang HJ (2010) Chem Eur J 16:6251–6256
6. Jana NR, Peng XG (2003) J Am Chem Soc 125:14280–14281
7. Pradhan N, Pal A, Pal T (2002) Colloids Surf A 196:247–257
8. Bharat B, Gregory JG, Michelle JA, Matthew EB (2013) Langmuir 29:4225–4234

9. Matthew D, Schaeublin NM, Farrington KE, Hussain SM, Johnson GR (2009) ACS Nano 3:984–994
10. Tang B, Li JL, Hou XL, Afrin T, Sun L, Wang XA (2013) Ind Eng Chem Res 52:4556–4563
11. Abhijith KS, Sharma R, Ranjan R, Thakur MS (2014) Photochem Photobiol Sci 13:986–991
12. Rai M, Yadav A, Gade A (2009) Biotechnol Adv 27:76–83
13. Deng ZW, Chen M, Wu LM (2007) J Phys Chem C 111:11692–11698
14. Tang DP, Yuan R, Chai YQ (2006) J Phys Chem B 110:11640–11646
15. Chen X, Zheng ZF, Ke XB, Jaatinen E, Xie TF, Wang DJ, Guo C, Zhao JC, Zhu HY (2010) Green Chem 12:414–419
16. Zheng NF, Stucky GD (2006) J Am Chem Soc 128:14278–14280
17. Ma L, Wang DS, Li JH, Bai BY, Fu LX, Li YD (2014) Appl Catal B 36–43:148–149
18. Liu L, Liu JC, Wang YJ, Yan X, Sun DD (2011) New J Chem 35:1418–1423
19. Li ZZ, Fan LJ, Zhang T, Li K (2011) J Hazard Mater 187:466–472
20. Motlagha AL, Bastani S, Hashemi MM (2014) Prog Org Coat 77:502–511
21. Zhang HJ, Chen GH (2009) Environ Sci Technol 43:2905–2910
22. Perkas N, Lipovsky A, Amirian G, Nitzan Y, Gedanken A (2013) J Mater Chem B 1:5309–5316
23. Li MH, Trevino MEN, Martinez NN, Jones CM, Wang JW (2009) Environ Sci Technol 43:2905–2910
24. Chen SF, Li JP, Qian K, Xu WP, Lu Y, Huang WX, Yu SH (2010) Nano Res 3:244–255
25. Zhong LS, Hu JS, Cui ZM, Wan LJ, Song WG (2007) Chem Mater 19:4557–4562
26. Liu R, Wang P, Wang XF, Yu HG, Yu JG (2012) J Phys Chem C 116:17721–17728
27. Zhang HJ, Li XY, Chen GH (2009) J Mater Chem 19:8223–8231
28. Zheng Z, Huang B, Qin X, Zhang X, Dai Y, Whangbo MH (2011) J Mater Chem 21:9079–9087
29. Bano I, Kumar RV, Hameed A (2012) Ionics 18:307–313
30. Zhang FX, Guan NJ, Li YZ, Zhang X, Chen JX, Zeng HS (2003) Langmuir 19:8230–8234
31. Chan SC, Barteau MA (2005) Langmuir 21:5588–5595
32. Mine E, Hirose M, Nagao D, Kobayashi Y, Konno M (2005) J Colloid Interface Sci 291:162–168
33. Zhang YY, Guo SB, Ma JQ, Ge HG (2014) J Sol-Gel Sci Technol 72:171–178
34. Guzman M, Dille J, Godet S (2012) Nanomed Nanotechnol Biol Med 8:37–45
35. Li G, Bai RB, Zhao XS (2008) Ind Eng Chem Res 47:8228–8232
36. Kosmulski M, Maczka E, Rosenholm JB (2002) J Phys Chem B 106:2918–2921
37. Li HB, Duan XC, Liu GC, Liu XQ (2008) J Mater Sci 43:1669–1676
38. Yang LB, Jiang X, Ruan WD, Yang JX, Zhao B, Xu WQ, Lombardi JR (2009) J Phys Chem C 113:16226–16231
39. Gerischer H, Heller A (1991) J Phys Chem 95:5261–5266
40. Sobana N, Muruganadham M, Swaminathan M (2006) J Mol Catal A 258:124–132
41. Liu HX, Cao YY, Peng HY, Qian HS, Yang XZ, Zhang HB (2014) CrystEngComm 16:2365–2370
42. Mandlimath TR, Gopal B (2011) J Mol Catal A 350:9–15